coatings

MDPI

Article

Carbon Dot-Titanium Dioxide (CD/TiO_2) Nanocomposites: Reusable Photocatalyst for Sustainable H_2 Production via Photoreforming of Green Organic Compounds

Pinelopi P. Falara [1,2], Maria Antoniadou [1,3,*], Adamantia Zourou [2], Elias Sakellis [1] and Konstantinos V. Kordatos [2,*]

[1] Institute of Nanoscience and Nanotechnology, National Center for Scientific Research "Demokritos", Agia Paraskevi, 15341 Athens, Greece; e.sakellis@inn.demokritos.gr (E.S.)
[2] School of Chemical Engineering, National Technical University of Athens, 9 Iroon Polytechniou St., Zografou, 15780 Athens, Greece
[3] Department of Chemical Engineering, University of Western Macedonia, 50100 Kozani, Greece
* Correspondence: mantoniadou@uowm.gr (M.A.); kordatos@central.ntua.gr (K.V.K.)

Abstract: The present work focuses on TiO_2 modification with carbon dots (CDs) using a hydrothermal process, which results in the synthesis of CD/TiO_2 nanocomposite photocatalysts characterized by exceptional optoelectronic properties. The structural and physicochemical properties of the obtained nanocomposites, which contained varying amounts of CDs, were precisely assessed. HR-TEM analysis showed that the prepared nanocomposites consisted of rod-shaped TiO_2 nanoparticles and CDs well-dispersed on their surface. The optical properties of the nanocomposites were studied using UV–vis diffuse reflectance spectroscopy. All CD/TiO_2 samples presented decreased energy gap values compared with bare TiO_2 samples; the band gap was further decreased as the CD concentration rose. Electrochemical measurements revealed that the presence of CDs improved the photocurrent response of the TiO_2, presumably due to enhanced charge separation and decreased recombination. The synthesized nanomaterials were used as photocatalysts to produce hydrogen via the photoreforming of ethanol and glycerol green organic compounds, under 1-sun illumination. The photocatalytic experiments confirmed that the optimum loading of CDs corresponded to a percentage of 3% (*w*/*w*). Ethanol photoreforming led to a H_2 production rate of 1.7 μmol·min^{-1}, while in the case of the glycerol sacrificial agent, the corresponding rate was determined to be 1.1 μmol·min^{-1}. The recyclability study revealed that the photocatalyst exhibited consistent stability during its reuse for hydrogen production in the presence of both ethanol and glycerol.

Keywords: carbon dots; photocatalysis; H_2 production; ethanol reforming; glycerol reforming

Citation: Falara, P.P.; Antoniadou, M.; Zourou, A.; Sakellis, E.; Kordatos, K.V. Carbon Dot-Titanium Dioxide (CD/TiO_2) Nanocomposites: Reusable Photocatalyst for Sustainable H_2 Production via Photoreforming of Green Organic Compounds. *Coatings* **2024**, *14*, 131. https://doi.org/10.3390/coatings14010131

Academic Editor: Gianfranco Carotenuto

Received: 19 December 2023
Revised: 13 January 2024
Accepted: 17 January 2024
Published: 19 January 2024

1. Introduction

The modern world faces critical challenges concerning the energy crisis and environmental pollution. Due to heavy reliance on fossil fuels, serious damage has been done to air quality from greenhouse gas emissions. The solution resides in transitioning to renewable energy sources, with solar energy emerging as the most promising clean energy on the earth because of its abundance, effectiveness, and easy large-scale utilization [1].

In recent years, the utilization of hydrogen (H_2) as a green fuel has emerged as a crucial change. This transition has stimulated the investigation of novel technologies such as aqueous phase reforming (APR). For example, the APR of crude glycerol contained in the wastewater streams of industrial facilities has been proposed as an alternative low-cost process, able to convert oxygenated molecules into H_2 [2,3]. Significant advancements in H_2 production have been achieved also via innovative methods that exploit solar light like photocatalysis and photoelectrocatalysis [1,4]. These advanced photoinduced processes appear to be effective in addressing the dual crisis of energy sustainability and environmental contamination.

Titanium dioxide (TiO_2) is considered the most promising semiconductor material used in photocatalytic applications (e.g., water splitting, waste water treatment, etc.); however, it suffers from a low utilization of visible light and high recombination reaction rate between photogenerated electrons and holes [5]. As it has been demonstrated, the activity of the TiO_2 photocatalyst for water splitting is significantly enhanced by incorporating noble metals. M. Saleh et al. [6] investigated the influence of the co-catalyst deposition and postulated that scarce elements and cost limitations for efficient large scale hydrogen production could be resolved via the optimization of loading Pt and Cu nanocrystals onto TiO_2. Furthermore, by introducing a ZIF-67-derived Co_3O_4@C metal-free co-catalyst onto TiO_2, the same group achieved the significantly enhancement of H_2 evolution rates via photocatalytic water splitting [7]. Another successful approach to TiO_2 modification in order to overcome these limitations was the fabrication of composite heterostructures with carbon-based nanomaterials such as carbon nanotubes (CNTs) [5,8,9], graphene oxide (GO) [10,11], reduced graphene oxide (r-GO) [12–15], graphitic carbon nitride (g-C_3N_4) [16,17], or more recently with carbon dots (CDs) [18,19]. CDs' structure involves a carbon core consisting mostly of sp^2 carbon domains connected by sp^3 carbon atoms and a large number of functional groups (-OH, -COOH, -NH_2, etc.) on the surface. Despite the limited number of studies that have been performed on the use of CDs in photocatalytic hydrogen production, they are a great sensitizer for TiO_2 photocatalysts as they are characterized by broad visible light absorption, efficient electron transfer properties, and high photostability. Additionally, CDs are capable of accepting photo-excited electrons generated by the TiO_2 semiconductor under illumination. Consequently, the separation of charge carriers is greatly enhanced as the recombination rate is reduced, which is crucial for efficient photocatalytic H_2 generation [20,21].

The recombination reaction rate may be significantly suppressed with the use of electron donor substances as sacrificial agents, due to the fact that they react irreversibly with the photogenerated holes and/or oxygen. For water as the target substance, the process results in simultaneous oxygen and hydrogen production. Nonetheless, the process of water cleavage is commonly regarded as having low efficiency. Photocatalytic reforming is more efficient for hydrogen production when using biomass-derived substances like ethanol and glycerol. The reforming of organic substances in the presence of water leads to the production of hydrogen and CO_2. Organic compounds such as organic acids [22], alcohols [23–25], amines [24,26,27], and sugars [28,29] are often employed as sacrificial agents. Photocatalytic hydrogen generation occurs simultaneously with the degradation of the organic compounds. In aqueous solutions under anaerobic conditions, the chemical reaction follows a reforming model, which involves the decomposition and mineralization of the organic compound, but also water decomposition and hydrogen production [30,31]. This is described by the following general scheme:

$$C_xH_yO_z + (2x - z)\,H_2O \rightarrow x\,CO_2 + \left(2x - z + \frac{y}{2}\right) H_2 \quad (1)$$

All the energy required for this endothermic reaction is provided by photons that are taken in by the photocatalyst. While photogenerated electrons reduce hydrogen ions and produce molecular hydrogen, photogenerated holes interact with the organic material and oxidize it [32].

In this work, CD/TiO_2 nanocomposites were synthesized through a simple and low-temperature procedure. More specifically, CDs were prepared using citric acid and urea precursors in a molar ratio of 1:100, following a domestic microwave-assisted synthesis for 4 min. To the best of our knowledge, this was the first time that as-prepared CDs have been combined with TiO_2 for photocatalytic H_2 generation. The structural and physicochemical properties of the obtained nanocomposites, which contained varying amounts of CDs, were thoroughly characterized. The prepared materials were then used as photocatalysts for hydrogen production using organic compounds as sacrificial agents. For this purpose, ethanol and glycerol have been tested and the amount of generated hydrogen under 1-sun

illumination was determined via gas chromatography. The obtained results confirmed that photocatalytic hydrogen production is strongly related to the nature and chemical structure of the organic substrate, the reaction conditions, and the CD content in the TiO_2 nanocomposite material. The aim of this work was to evaluate the potential of novel and low-cost CD/TiO_2 nanocomposites in the field of photocatalytic H_2 generation. It is important to note that for this application, green liquid organic hydrogen carrier systems (ethanol and glycerol) were utilized. Consequently, this study laid the foundation for the achievement of sustainable H_2 production using renewables (from/using biomass-derived compounds and solar light).

2. Materials and Methods

2.1. Materials

All chemicals of analytical grade were used as received. Urea was obtained from Sigma-Aldrich (St. Louis, MO, USA); citric acid was purchased from Fluka and glycerol (≥99%) from Carlo Erba (Cornaredo, Italy). The nanocrystalline TiO_2 used in the present work was commercial Degussa P25. Absolute ethanol (C_2H_6O, ≥99%) was purchased from Acros-Organics (Geel, Belgium). Perfluorinated Nafion ($C_7HF_{13}O_5S{\cdot}C_2F_4$, ≥98%) was obtained from Chem-Lab (Zedelgem, Belgium) and sodium hydroxide (NaOH) from Merck (Darmstadt, Germany). Deionized (DI) water was used throughout.

2.2. Synthesis of the CD/TiO_2 Nanocomposites

The CDs were prepared following a domestic microwave-assisted synthesis, constituting a bottom–up strategy. In this method, 0.1 g of citric acid and 3.12 g of urea were used as CD precursors. Specifically, a molar ratio of citric acid:urea of 1:100 was added to 10 mL of DI water [33]. The mixture was vigorously stirred for about 10 min and then was placed in a domestic microwave for 4 min. After natural cooling, the resulting product was dissolved in DI water and was centrifuged at 6000 rpm for 30 min and filtrated in order to separate the CD solution from by-products. Thus, the precipitate was removed, while the supernatant dispersion of the CDs was solidified with freeze-drying technology, and the resulting powder of the CDs was soft and light. The main steps of the synthesis route of the CDs are shown in Figure 1.

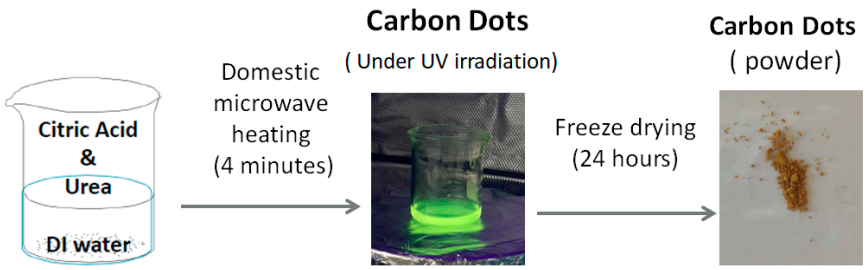

Figure 1. CD synthesis procedure diagram.

Regarding the CD/TiO_2 nanocomposites, they were obtained with a hydrothermal method. More specifically, 20 mL of distilled water and 6 mL of ethanol were mixed together, and then 400 mg of Degussa P25 and 4 mL of CDs dispersed in ethanol were added. The concentration of the CDs' dispersion varied in order to produce nanocomposites with different concentrations of CDs. To examine the influence of the content on photocatalytic H_2 production, 1, 2, 3, and 4% *w*/*w* CD/TiO_2 nanocomposites were synthesized. The reaction mixture was stirred for 30 min at room temperature in order to achieve homogeneity and then transferred into a Teflon-sealed autoclave and heated at 140 °C for 4 h [34]. The resulting photocatalysts were washed with DI water three times, collected with centrifugation, and dried at 80 °C overnight.

2.3. Photoelectrodes

The fabrication of the working electrode followed the subsequent steps: transparent FTO conductive glass electrodes (7 ohms cm^{-2}, Pilkington, Lathom, UK) underwent a thorough cleaning with a solution composed of 2% Hellmanex in water, followed by washing with ethanol and acetone. To prepare the photoelectrode, 10 mg of each photocatalyst was dispersed in a solution comprising 50 µL of Nafion perfluorinated solution, 290 µL of 3D water, and 168 µL of absolute ethanol. The resulting suspensions were ground and doctor-bladed onto the FTO electrode, forming a uniform coating. Subsequently, the samples were heated at 200 °C for 1 h.

2.4. Characterization Methods

X-ray powder diffraction (XRD) analysis was performed using a D8 Advance diffractometer, operating with Bragg–Brentano geometry with Cu $K_{\alpha1}$ (λ = 1.5406 Å) and Cu $K_{\alpha2}$ (λ = 1.5444 Å) radiation (Bruker, Billerica, MA, USA). Data were collected over the angular range of 10 to 80°, counting for 2 s at each step of 0.02° in the detector position.

Fourier transform infrared (FT-IR) spectra were obtained using a Jasco FTIR 4200 spectrometer in the range of 400–4000 cm^{-1} using KBr pellets (Jasco, Tokyo, Japan).

The nanostructure was studied with a FEI Talos F200i field-emission (scanning) transmission electron microscope (S/TEM) operating at 200 keV, equipped with a windowless energy-dispersive spectroscopy microanalyzer (6T/100 Bruker). The TEM samples were prepared by suspending the nanoparticles in ethanol and the subsequent evaporation in air using a suspension droplet on a holey carbon film supported by a copper grid.

The optical properties of the samples were analyzed with UV–vis diffuse reflectance spectroscopy, using a Hitachi 3010 spectrophotometer equipped with a 60 mm diameter integrating sphere, and $BaSO_4$ was used as a reference. The absorption data were expressed with Kubelka–Munk units using the respective equation (F(R)).

The electrochemical characterization of the samples was performed via an Autolab potentiostat (PGSTAT-302N). Photocurrent-time (I-t) characteristics were obtained at open-circuit potential, utilizing a two-electrode system and an illuminated (active) area of 3 cm^2. Platinum foil (Pt) was employed as the counter electrode. The solution used for the electrochemical measurements contained 25% v/v ethanol, 0.5 M sodium hydroxide (NaOH), and the illumination source was simulated solar light (1 sun, 1000 Wm^{-2}) from a Xenon 300 W source.

2.5. Photocatalytic Setup for Hydrogen Production and Detection

A cylindrical reactor was used, made of Pyrex glass, with carrying fittings allowing for gas inlet–outlet. The reactor was illuminated with a 300 W Xenon lamp (Oriel) and placed at a distance of 10 cm. The detection of hydrogen was realized via an SRI 8610C gas chromatograph with Ar as the carrier gas. Calibration of the gas chromatograph signal was carried out using a standard mixture of 0.25% v/v H_2 in Ar. The intensity of radiation at the position of the reactor was measured with an Oriel Radiant Power Meter. Samples were periodically collected using an automatic gas sampling valve and the exact concentration of hydrogen in the reactor effluent was measured as a function of time of illumination. For each experiment, 200 mg of the photocatalysts were dispersed in 100 mL of an aqueous solution containing a certain amount of the organic compound used as a sacrificial agent. When ethanol was used as a sacrificial agent, the concentration was 25% v/v; when glycerol was tested, the concentration was 10% v/v. The ethanol and glycerol concentrations were identified as optimal based on their performance in promoting efficient hydrogen production across various photocatalytic processes [35–43]. The reproducibility of the experiments was studied, and the results are presented in Figure S4. During all the experiments, stirring was continuous. Firstly, the solution was degassed with an Ar flow, and then the lamp was switched on.

3. Results and Discussion

3.1. Photocatalyst Characterization

The CD/TiO_2 nanocomposite photocatalysts were characterized using XRD, FT-IR, and TEM techniques. The results revealed the presence of graphitic carbon in the nanocomposite material and confirmed the uniform dispersal of the CDs on the surface of TiO_2.

The structural properties of the synthesized materials were examined through XRD analysis. The characteristic peaks of TiO_2 P25, which consists of a mixture of anatase (A) (JCPDS 21-1272) and rutile (R) (JCPDS 21-1276) nanocrystals [44], were clearly visible in both patterns, as shown in Figure 2a. More specifically, the observed diffraction peaks at 2θ: 25.24°, 27.39°, 35.90°, 36.84°, 37.72°, 38.60°, 41.10°, 48.00°, 53.91°, 55.03°, 56.66°, 62.56°, 68.87°, 70.35°, and 74.98° were assigned to the A(101), R(110), R(101), A(103), A(004), A(112), R(111), A(002), A(105), R(221), A(211), R(220), A(204), A(116), A(220), and A(215) planes, respectively [45,46]. Concerning the XRD pattern of the CD/TiO_2, the absence of the characteristic signal at 13° for the CDs [47] indicated their quantum-sized dimensions, low content, and uniform, high dispersion on the TiO_2 surface [48,49]. The results of the characterization of the synthesized materials using the FT-IR technique, used to clarify their chemical structure, are presented in Figure 2b. The broad characteristic band in the region above 3000 cm^{-1} was assigned to the water molecules absorbed on the surface and surface hydroxyl groups. FTIR spectra of the CDs and CD/TiO_2 exhibited a band around 1700 cm^{-1} indicating the presence of C=O bonds. The broad absorption band of the CD/TiO_2 nanocomposite below 1000 cm^{-1} became wider compared with that of the pure TiO_2, which was attributed to the combination of the Ti–O–Ti and Ti–O–C vibrations. It is important to note that the XRD and FT-IR results of the CD/TiO_2 presented here specifically pertain to the 3% *w*/*w* CD/TiO_2 composition. The XRD and FT-IR spectra of 1, 2, as well as 4% *w*/*w* CD/TiO_2 are presented in Figures S1 and S2, respectively.

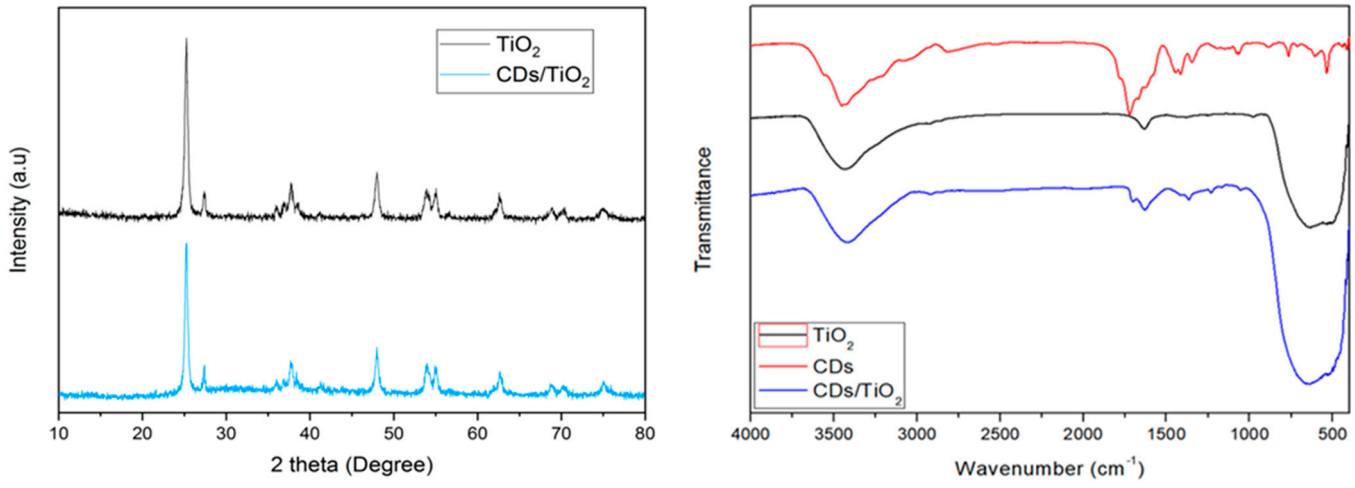

Figure 2. (**a**) XRD diffraction patterns of TiO_2 and CD/TiO_2 film; (**b**) FT-IR spectra of pristine TiO_2 and the synthesized materials.

To elucidate the morphology of the CD/TiO_2 nanocomposite, HR-TEM measurement was conducted. The HR-TEM images (Figure 3) demonstrated the existence of nanoparticles with an average size less than 20 nm. Figure 3a,b demonstrate that the TiO_2 nanoparticles were rod-shaped and the CDs were well-dispersed on their surface. Lattice fringes can be clearly seen in the high-resolution image (Figure 3c,d). The spacing between the adjacent lattice fringes was measured to be 0.189 and 0.333 nm, corresponding to the interplanar distance of the (200) planes in the typical anatase phase (TiO_2) and to the (002) spacing of the graphitic carbon (CDs), respectively.

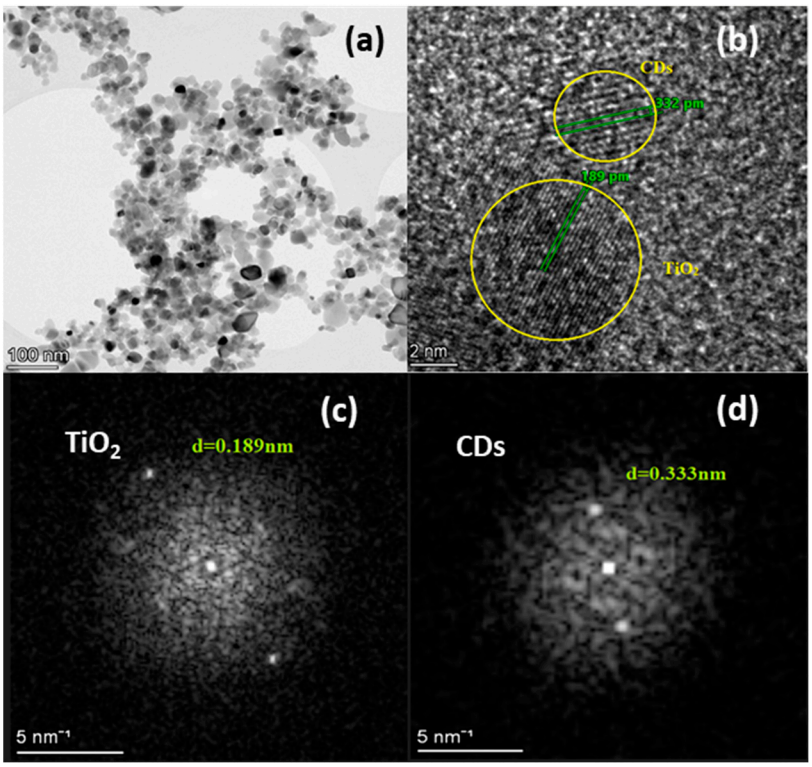

Figure 3. (**a**) TEM image of CD/TiO_2 nanocomposite at a magnification scale of 100 nm; (**b**) HR-TEM image of the CD/TiO_2 nanocomposite at a magnification scale of 10 nm, where lattice fringes of TiO_2 and CDs are depicted, as are fast Fourier transform (FFT) patterns of (**c**) TiO_2 and (**d**) CDs.

In order to study the optical properties of the nanocomposites, the DR/UV–vis spectra plotted as the Kubelka–Munk function of the reflectance F(R) versus the energy of exciting light for the samples are shown in Figure 4.

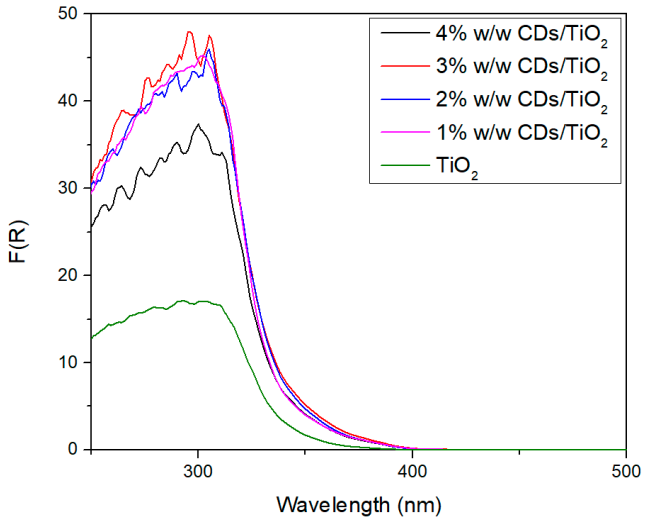

Figure 4. UV–vis/DR spectra plotted as the Kubelka–Munk function of the reflectance F(R).

The band-gap energies of the samples were estimated from the tangent lines in the plots of the modified Kubelka–Munk function [50,51]. A remarkable change in the DR/UV-vis spectra for the containing CDs could be observed, which suggested that they reflected significantly less light than the bare TiO_2-P25. This outcome showed great potential as it indicated an enhanced scattering of photons due the presence of CDs, leading to an improved light-harvesting efficiency. More specifically, the calculated band gaps of the

samples with TiO_2, 1% *w*/*w* CD/TiO_2, 2% *w*/*w* CD/TiO_2, 3% *w*/*w* CD/TiO_2, and 4% *w*/*w* CD/TiO_2 were 3.39, 3.26, 3.24, 3.18, and 3.13 eV, respectively.

The photo-electrochemical properties of the nanocomposites deposited on the FTO electrodes were examined in 0.5 M NaOH under 1-sun illumination conditions.

To evaluate the photoelectric response of the catalysts, the transient photocurrent responses, in order to study the photocatalytic effect, were used (I-t). Figure 5 shows the photocurrent response of the CD/TiO_2 thin films of various concentrations under 1-sun illumination conditions. As expected, each of the CD/TiO_2 nanocomposites produced photocurrents upon illumination, which decreased to zero when the illumination was off. Even though the presence of CDs could improve the photocurrent response of the TiO_2, presumably due to enhancing charge separation and decreasing recombination, as shown in Figure 5, a stable but low photocurrent response, due to the quick recombination of photo-generated electrons and holes and the weak response of visible light, was presented for the samples with 1% *w*/*w* CD/TiO_2 and 2% *w*/*w* CD/TiO_2. The sample with 3% *w*/*w* CD/TiO_2 demonstrated a heightened anodic photocurrent response. This could be attributed to the increased absorption of visible light and improved charge separation, both enhanced by the higher concentration of CDs. However, a further increase in CD concentration, beyond 3% *w*/*w*, did not improve the photocurrent values (4% *w*/*w* CD/TiO_2); instead, the photocurrent density decreased. This observation suggested that an excessive CD content may block the active surface area. This was probably due to the opacity and light scattering of the CDs decreasing the absorption of the incident light. As a consequence, the photocurrent response was reduced [34].

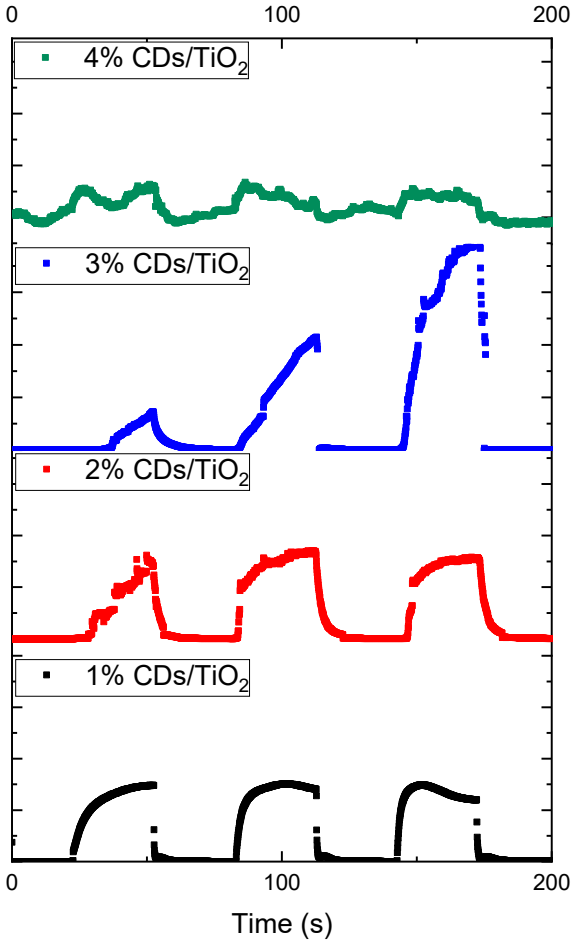

Figure 5. On–off photocurrent density–time curves of the CD/TiO_2 nanocomposites obtained at Voc in 0.5 M NaOH and 25% *v*/*v* ethanol.

3.2. Photocatalytic Hydrogen Production with Ethanol and Glycerol Reforming

Photocatalytic hydrogen generation consistently occurred in all the CD/TiO_2 photocatalysts with varying CD contents. Conversely, in the case of bare TiO_2, no hydrogen production was observed.

The temporal evolution of H_2 in the presence of CD/TiO_2 photocatalysts is shown in Figure 6. In each experiment, 200 mg of the corresponding photocatalyst was added in a 100 mL aqueous solution containing the organic substrate. In the presence of 25% *v*/*v* ethanol, the obtained data are shown in Figure 6a as a function of the CDs' percentage and reaction time. The results revealed that there was no H_2 production in the case of pure Degussa P25; however, all of the prepared nanocomposite photocatalysts exhibited satisfying hydrogen production rates. Four different loadings of CDs were tested in order to clarify which was optimal. The sample containing 3% *w*/*w* CDs demonstrated the highest H_2 production rate, reaching the value of 1.7 μmol H_2/min. In every curve, there was a section of the initial incline, representing the period required for hydrogen accumulation within the reaction mixture and its transport through the tubing to the detection area, and the peak rate, which served as an indicator of the maximum possible hydrogen production rate under the present conditions. The presence or absence of a plateau depended on the balance between the amount of photocatalysts and fuel, as well as the intensity of incident radiation.

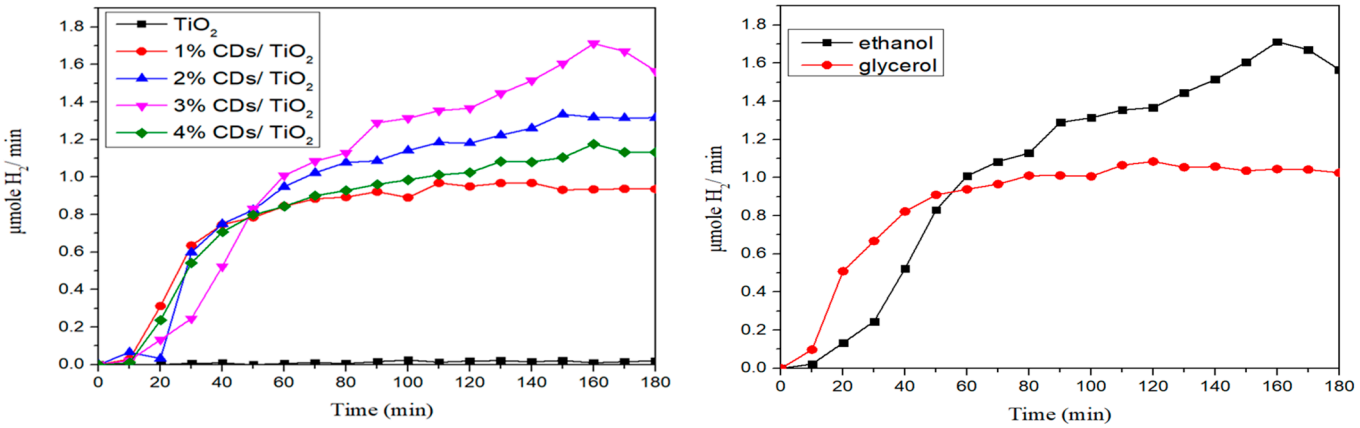

(**a**) (**b**)

Figure 6. Photocatalytic evolution of hydrogen with (**a**) ethanol reforming in the presence of CD/TiO_2 nanocomposites under 1-sun illumination and (**b**) ethanol and glycerol reforming in the presence of 3% *w*/*w* CD/TiO_2 nanocomposites under 1-sun illumination.

The nanocomposite that exhibited superior behavior in photocatalytic hydrogen production via ethanol reforming (i.e., 3% *w*/*w* CD/TiO_2) was studied using another organic substance as a sacrificial agent. The data of Figure 6b were obtained with a 10% *v*/*v* glycerol in a 100 mL aqueous solution. Following a similar experimental procedure, it was proven that the use of ethanol as a sacrificial agent exhibited better H_2 production rates than the use of glycerol. To be more precise, the maximum hydrogen production rate observed with glycerol was approximately 1.1 μmol $H_2 \cdot min^{-1}$, which was lower when compared to ethanol's rate of 1.7 μmol $H_2 \cdot min^{-1}$.

The stability and recyclability of the CD/TiO_2 photocatalysts were also investigated through the cycling experiments that are exhibited in Figure 7. More specifically, a 3% *w*/*w* CD/TiO_2 photocatalyst was used for three consecutive cycles in the presence of each sacrificial agent (ethanol and glycerol). Each cycle was carried out under the exact same conditions mentioned in Section 2.5. After each test, the photocatalyst was thoroughly washed with DI water. The recyclability study revealed that the photocatalyst exhibited consistent stability during its reuse for hydrogen production from both ethanol and glycerol. However, in both cases, there was an increment in the second cycle. This may have been

due to the formation of intermediates during the process, which possibly enhanced the nanocomposite's photocatalytic activity [52]. It is worth mentioning that the XRD spectra of the CD/TiO_2 nanocomposites after the utilization of three consecutive cycles are presented in Figure S3. Based on the XRD results, there were no alterations in the crystal structure of the sample, proving the photocatalyst's high stability.

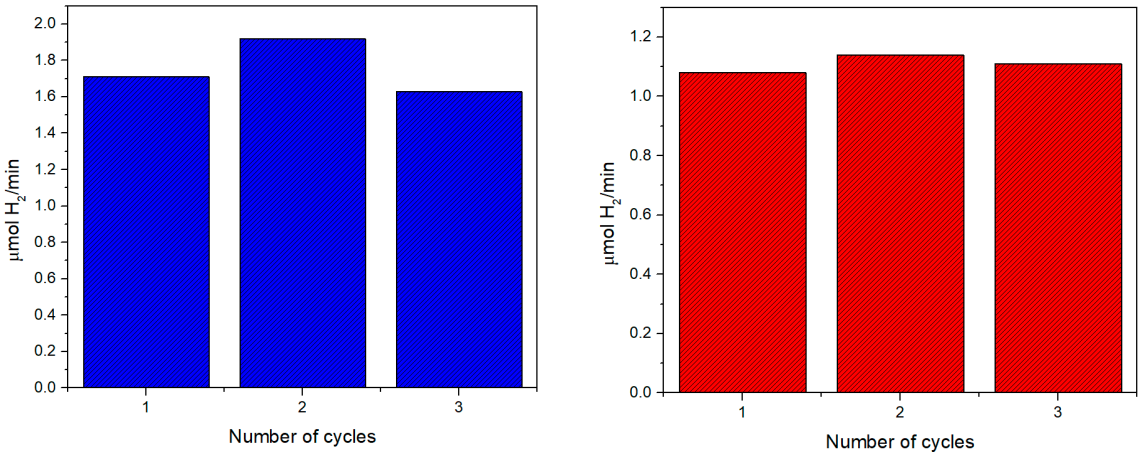

Figure 7. Recyclability tests of 3% *w*/*w* CD/TiO_2 in the presence of (**a**) 25% *v*/*v* ethanol and (**b**) 10% *v*/*v* glycerol.

Furthermore, in order to highlight the novelty and advancements of this study regarding photocatalytic hydrogen production, a survey of TiO_2-based photocatalysts within the recent literature was conducted. The comparisons between them, which is presented in Table 1, intended to clarify the contribution made within this field and distinguish the results from the existing literature.

Table 1. Comparison of TiO_2-based photocatalysts for hydrogen production in the recent literature.

Catalyst	Cocatalyst	Sacrificial Agent	Maximum Hydrogen Production Rate	Ref.
CD/TiO_2	-	25% *v*/*v* ethanol	1.7 μmol/min 102 μmol/h or 510 μmol/(h·g)	This work
	-	25% *v*/*v* methanol	9.8 μmol/h	[53]
	- Pt	0.3 M triethanolamine	472 μmol/(h·g) 1458 μmol/(h·g)	[54]
CD/g-C_3N_4/TiO_2	Pt	10% *v*/*v* triethanolamine	580 μmol/(h·g)	[55]
g-C_3N_4/TiO_2	-	20% *v*/*v* methanol	110 μmol/(h·g)	[56]
Black phosphorus quantum dot/TiO_2	-	20% *v*/*v* methanol	112 μmol/(h·g)	[57]
$MoSe_2$/TiO_2	-	30% *v*/*v* methanol	401 μmol/(h·g)	[58]
Red phosphorus/TiO_2	Pt	-	215.5 μmol/(h·g)	[59]

4. Conclusions

In summary, this work was focused on the synthesis and characterization of CD/TiO_2 nanocomposite material, as well as the evaluation of its performance in photocatalytic hydrogen production. As it is known, TiO_2 semiconductors suffer from the low utilization of visible light and a high recombination reaction rate between photogenerated electrons

and holes. In order to overcome these drawbacks, its combination with CDs has been suggested. CDs, characterized by broad visible light absorption, efficient electron transfer properties, and high photostability, are among the most promising candidates for the sensitization of TiO_2 photocatalysts. Herein, a facile and novel synthetic route is presented for the first time. More specifically, a three-step process was followed for the preparation of CD/TiO_2, where CDs were first prepared with a rapid domestic microwave-assisted synthesis, followed by freeze drying. Then, a facile hydrothermal process using the as-prepared CDs and TiO_2 as precursors was conducted. The obtained CD/TiO_2 sample could be easily coated onto conductive substrates to form thin films, which could be applied in various applications. The aim of this study was the investigation of the CD concentration effect on the photocatalytic performance for hydrogen production. Therefore, four different concentrations of CDs (1% *w*/*w*, 2% *w*/*w*, 3% *w*/*w*, and 4% *w*/*w*) were evaluated. The physicochemical properties of the samples were studied via XRD, FT-IR, HR-TEM/FFT, UV–Vis, as well as photo-electrochemical measurements (I-t). More specifically, based on the XRD results, the absence of diffraction peaks in the CDs was attributed to their extremely small size and their uniform distribution onto the TiO_2 surface. Additionally, the absorption peak of 1700 cm^{-1} in the FT-IR spectra, which was attributed to the C=O stretching vibrations due to the presence of CDs in the nanocomposite material, increased when the CD concentration also increased. Regarding the morphology study of the nanocomposite, the TiO_2 nanoparticles were rod-shaped while the CDs were well-dispersed onto their surface. Moreover, it is important to note that all CD/TiO_2 samples presented decreased energy gap values compared to TiO_2; the band gap further decreased as the CD concentration rose. Similarly, the photocurrent response was enhanced as the CD concentration increased to a specific limit, where CDs could block the active surface area; this may have been due to opacity and light scattering, resulting in the decrease in incident light absorption. Finally, the performance of the as-prepared CD/TiO_2 photocatalysts containing varying amounts of CDs was evaluated in their capability to produce H_2, using green organic solvents (e.g., ethanol and glycerol) as sacrificial agents. All of the as-prepared nanocomposite photocatalysts exhibited satisfying hydrogen production rates, as opposed to the bare TiO_2. Among all the samples, the one containing 3% *w*/*w* CDs demonstrated the highest H_2 production rate reaching the value of 1.7 μmol H_2/min and 1.1 μmol H_2/min in the presence of ethanol and glycerol, respectively. The fact that the 3% *w*/*w* CD/TiO_2 exhibited the best photocatalytic performance corresponded with the photo-electrochemical measurements, as mentioned above. The high recyclability and stability of the 3% *w*/*w* CD/TiO_2 were confirmed after its utilization for three cycles reaching the value of 1.63 μmole H_2/min and 1.11 μmole H_2/min after the last cycle for ethanol and glycerol, respectively, while its crystal structure presented no alterations.

Supplementary Materials: The following supporting information can be downloaded at: https://www.mdpi.com/article/10.3390/coatings14010131/s1, Figure S1. XRD spectra of the 1% *w*/*w* CD/TiO_2, 2% *w*/*w* CD/TiO_2, and 4% *w*/*w* CD/TiO_2; Figure S2. FT-IR spectra of the 1% *w*/*w* CD/TiO_2, 2% *w*/*w* CD/TiO_2, and 4% *w*/*w* CD/TiO_2; Figure S3. XRD spectra of the 3% *w*/*w* CD/TiO_2 before and after utilization; Figure S4. Results of the 3% *w*/*w* CD/TiO_2 reproducibility in the presence of 25% *v*/*v* ethanol.

Author Contributions: Conceptualization, M.A.; methodology P.P.F., M.A. and K.V.K.; validation, P.P.F. and M.A.; formal analysis, P.P.F. and M.A.; investigation, P.P.F., M.A., A.Z., E.S. and K.V.K.; resources, P.P.F., M.A. and K.V.K.; data curation, M.A.; writing—original draft preparation, P.P.F. and A.Z.; writing—review and editing, P.P.F., M.A. and K.V.K.; visualization, P.P.F., A.Z. and M.A.; supervision, M.A. and K.V.K.; project administration, M.A.; funding acquisition, P.P.F. and M.A. All authors have read and agreed to the published version of the manuscript.

Funding: This research was funded by the Hellenic Foundation for Research and Innovation (HFRI) and the General Secretariat for Research and Technology (GSRT), under grant agreement number 2490 and the European Union's H2020 Programme iWAYS, under grant agreement number 958274.

Institutional Review Board Statement: Not applicable.

Informed Consent Statement: Not applicable.

Data Availability Statement: Data are contained within the article and supplementary materials.

Conflicts of Interest: The authors declare no conflicts of interest. The funders had no role in the design of the study; in the collection, analyses, or interpretation of data; in the writing of the manuscript; or in the decision to publish the results.

References

1. Li, Z.; Fang, S.; Sun, H.; Chung, R.J.; Fang, X.; He, J.H. Solar Hydrogen. *Adv. Energy Mater.* **2023**, *13*, 2203019. [CrossRef]
2. Zoppi, G.; Pipitone, G.; Pirone, R.; Bensaid, S. Aqueous Phase Reforming Process for the Valorization of Wastewater Streams: Application to Different Industrial Scenarios. *Catal. Today* **2022**, *387*, 224–236. [CrossRef]
3. Coronado, I.; Stekrova, M.; Reinikainen, M.; Simell, P.; Lefferts, L.; Lehtonen, J. A Review of Catalytic Aqueous-Phase Reforming of Oxygenated Hydrocarbons Derived from Biorefinery Water Fractions. *Int. J. Hydrogen Energy* **2016**, *41*, 11003–11032. [CrossRef]
4. Pitchaimuthu, S.; Sridharan, K.; Nagarajan, S.; Ananthraj, S.; Robertson, P.; Kuehnel, M.F.; Irabien, Á.; Maroto-Valer, M. Solar Hydrogen Fuel Generation from Wastewater—Beyond Photoelectrochemical Water Splitting: A Perspective. *Energies* **2022**, *15*, 7399. [CrossRef]
5. Nguyen, H.A.; Pham, T.N.; Le, N.T.T.; Huynh, L.T.N.; Nguyen, T.T.T.; Vo, Q.K.; Nguyen, T.H.; Le, V.H.; Nguyen, T.T.T.; Nguyen, T.T.; et al. Nanocomposite TiO_2@CNTs for High-Voltage Symmetrical Supercapacitor in Neutral Aqueous Media. *J. Solid State Electrochem.* **2023**, *27*, 2811–2820. [CrossRef]
6. Saleh, M.; Abdelhamid, H.N.; Fouad, D.M.; El-Bery, H.M. Enhancing Photocatalytic Water Splitting: Comparative Study of TiO_2 Decorated Nanocrystals (Pt and Cu) Using Different Synthesis Methods. *Fuel* **2023**, *354*, 129248. [CrossRef]
7. El-Bery, H.M.; Abdelhamid, H.N. Photocatalytic Hydrogen Generation via Water Splitting Using ZIF-67 Derived Co_3O_4@C/TiO_2. *J. Environ. Chem. Eng.* **2021**, *9*, 105702. [CrossRef]
8. Ren, Y.; Chen, Y.; Li, Q.; Li, H.; Bian, Z. Microwave-Assisted Photocatalytic Degradation of Organic Pollutants via CNTs/TiO_2. *Catalysts* **2022**, *12*, 940. [CrossRef]
9. Nguyen, H.P.; Cao, T.M.; Nguyen, T.T.; Van Pham, V. Improving Photocatalytic Oxidation of Semiconductor (TiO_2, SnO_2, ZnO)/CNTs for NO_x Removal. *J. Ind. Eng. Chem.* **2023**, *127*, 321–330. [CrossRef]
10. Kumaran, V.; Sudhagar, P.; Konga, A.K.; Ponniah, G. Photocatalytic Degradation of Synthetic Organic Reactive Dye Wastewater Using GO-TiO_2 Nanocomposite. *Polish J. Environ. Stud.* **2020**, *29*, 1683–1690. [CrossRef]
11. Rajoria, S.; Vashishtha, M.; Sangal, V.K. Electrochemical Treatment of Electroplating Wastewater Using Synthesized GO/TiO_2 Nanotube Electrode. *Environ. Sci. Pollut. Res.* **2023**, *30*, 71226–71251. [CrossRef]
12. Jagadeesh, B.S.; Muniyappa, M.; Navakoteswara Rao, V.; Mudike, R.; Shastri, M.; Tathagata, S.; Shivaramu, P.D.; Shankar, M.V.; Ananda Kumar, C.S.; Rangappa, D. Enhanced Photocatalytic Hydrogen Evolution from Reduced Graphene Oxide-Defect Rich TiO_{2-x} Nanocomposites. *Int. J. Hydrogen Energy* **2022**, *47*, 40242–40253. [CrossRef]
13. Liu, S.; Jiang, T.; Fan, M.; Tan, G.; Cui, S.; Shen, X. Nanostructure Rod-like TiO_2-Reduced Graphene Oxide Composite Aerogels for Highly-Efficient Visible-Light Photocatalytic CO_2 Reduction. *J. Alloys Compd.* **2021**, *861*, 158598. [CrossRef]
14. Fei, Y.; Ye, X.; Al-Baldawy, A.S.; Wan, J.; Lan, J.; Zhao, J.; Wang, Z.; Qu, S.; Hong, R.; Guo, S.; et al. Enhanced Photocatalytic Performance of TiO_2 Nanowires by Substituting Noble Metal Particles with Reduced Graphene Oxide. *Curr. Appl. Phys.* **2022**, *44*, 33–39. [CrossRef]
15. John, D.; Jose, J.; Bhat, S.G.; Achari, V.S. Integration of Heterogeneous Photocatalysis and Persulfate Based Oxidation Using TiO_2-Reduced Graphene Oxide for Water Decontamination and Disinfection. *Heliyon* **2021**, *7*, e07451. [CrossRef]
16. Ibrahim, I.; Belessiotis, G.V.; Antoniadou, M.; Kaltzoglou, A.; Sakellis, E.; Katsaros, F.; Sygellou, L.; Arfanis, M.K.; Salama, T.M.; Falaras, P. Silver Decorated TiO_2/g-C_3N_4 Bifunctional Nanocomposites for Photocatalytic Elimination of Water Pollutants under UV and Artificial Solar Light. *Results Eng.* **2022**, *14*, 100470. [CrossRef]
17. Ratshiedana, R.; Kuvarega, A.T.; Mishra, A.K. Titanium Dioxide and Graphitic Carbon Nitride–Based Nanocomposites and Nanofibres for the Degradation of Organic Pollutants in Water: A Review. *Environ. Sci. Pollut. Res.* **2021**, *28*, 10357–10374. [CrossRef]
18. Falara, P.P.; Ibrahim, I.; Zourou, A.; Sygellou, L.; Sanchez, D.E.; Romanos, G.E.; Givalou, L.; Antoniadou, M.; Arfanis, M.K.; Han, C.; et al. Bi-Functional Photocatalytic Heterostructures Combining Titania Thin Films with Carbon Quantum Dots (C-QDs/TiO_2) for Effective Elimination of Water Pollutants. *Environ. Sci. Pollut. Res.* **2023**, *30*, 124976–124991. [CrossRef]
19. Huang, X.; Sun, L.; Liu, X.; Ge, M.; Zhao, B.; Bai, Y.; Wang, Y.; Han, S.; Li, Y.; Han, Y.; et al. Increase and Enrichment of Active Electrons by Carbon Dots Induced to Improve TiO_2 Photocatalytic Hydrogen Production Activity. *Appl. Surf. Sci.* **2023**, *630*, 157494. [CrossRef]
20. Sendão, R.M.S.; Esteves da Silva, J.C.G.; Pinto da Silva, L. Photocatalytic Removal of Pharmaceutical Water Pollutants by TiO_2—Carbon Dots Nanocomposites: A Review. *Chemosphere* **2022**, *301*, 134731. [CrossRef]
21. Vyas, Y.; Chundawat, P.; Dharmendra, D.; Punjabi, P.B.; Ameta, C. Review on Hydrogen Production Photocatalytically Using Carbon Quantum Dots: Future Fuel. *Int. J. Hydrogen Energy* **2021**, *46*, 37208–37241. [CrossRef]

22. Alsalka, Y.; Al-Madanat, O.; Curti, M.; Hakki, A.; Bahnemann, D.W. Photocatalytic H_2 Evolution from Oxalic Acid: Effect of Cocatalysts and Carbon Dioxide Radical Anion on the Surface Charge Transfer Mechanisms. *ACS Appl. Energy Mater.* **2020**, *3*, 6678–6691. [CrossRef]
23. Vitiello, G.; Clarizia, L.; Abdelraheem, W.; Esposito, S.; Bonelli, B.; Ditaranto, N.; Vergara, A.; Nadagouda, M.; Dionysiou, D.D.; Andreozzi, R.; et al. Near UV-Irradiation of CuO_x-Impregnated TiO_2 Providing Active Species for H_2 Production Through Methanol Photoreforming. *ChemCatChem* **2019**, *11*, 4314–4326. [CrossRef]
24. Tang, J.H.; Sun, Y. Visible-Light-Driven Organic Transformations Integrated with H_2production on Semiconductors. *Mater. Adv.* **2020**, *1*, 2155–2162. [CrossRef]
25. Wang, L.; Geng, X.; Zhang, L.; Liu, Z.; Wang, H.; Bian, Z. Effects of Various Alcohol Sacrificial Agents on Hydrogen Evolution Based on CoS_2@SCN Nanomaterials and Its Mechanism. *Chemosphere* **2022**, *286*, 131558. [CrossRef]
26. Pantoja-Espinoza, J.C.; Domínguez-Arvizu, J.L.; Jiménez-Miramontes, J.A.; Hernández-Majalca, B.C.; Meléndez-Zaragoza, M.J.; Salinas-Gutiérrez, J.M.; Herrera-Pérez, G.M.; Collins-Martínez, V.H.; López-Ortiz, A. Comparative Study of Zn_2 Ti_3 O_8 and $ZnTio_3$ Photocatalytic Properties for Hydrogen Production. *Catalysts* **2020**, *10*, 1372. [CrossRef]
27. Muscetta, M.; Clarizia, L.; Garlisi, C.; Palmisano, G.; Marotta, R.; Andreozzi, R.; Di Somma, I. Hydrogen Production upon UV-Light Irradiation of Cu/TiO_2 Photocatalyst in the Presence of Alkanol-Amines. *Int. J. Hydrogen Energy* **2020**, *45*, 26701–26715. [CrossRef]
28. Toledo-Camacho, S.Y.; Rey, A.; Maldonado, M.I.; Llorca, J.; Contreras, S.; Medina, F. Photocatalytic Hydrogen Production from Water-Methanol and -Glycerol Mixtures Using Pd/TiO_2(-WO_3) Catalysts and Validation in a Solar Pilot Plant. *Int. J. Hydrogen Energy* **2021**, *46*, 36152–36166. [CrossRef]
29. Alvarado-Ávila, M.I.; De Luca, S.; Edlund, U.; Ye, F.; Dutta, J. Cellulose as Sacrificial Agents for Enhanced Photoactivated Hydrogen Production. *Sustain. Energy Fuels* **2023**, *7*, 1981–1991. [CrossRef]
30. Yao, Y.; Gao, X.; Li, Z.; Meng, X. Photocatalytic Reforming for Hydrogen Evolution: A Review. *Catalysts* **2020**, *10*, 335. [CrossRef]
31. Yan, Z.; Yin, K.; Xu, M.; Fang, N.; Yu, W.; Chu, Y.; Shu, S. Photocatalysis for Synergistic Water Remediation and H_2 Production: A Review. *Chem. Eng. J.* **2023**, *472*, 145066. [CrossRef]
32. Lianos, P.; Strataki, N.; Antoniadou, M. Photocatalytic and Photoelectrochemical Hydrogen Production by Photodegradation Of organic Substances. *Pure Appl. Chem.* **2009**, *81*, 1441–1448. [CrossRef]
33. Stachowska, J.D.; Murphy, A.; Mellor, C.; Fernandes, D.; Gibbons, E.N.; Krysmann, M.J.; Kelarakis, A.; Burgaz, E.; Moore, J.; Yeates, S.G. A Rich Gallery of Carbon Dots Based Photoluminescent Suspensions and Powders Derived by Citric Acid/Urea. *Sci. Rep.* **2021**, *11*, 10554. [CrossRef]
34. Yu, H.; Zhao, Y.; Zhou, C.; Shang, L.; Peng, Y.; Cao, Y.; Wu, L.Z.; Tung, C.H.; Zhang, T. Carbon Quantum Dots/TiO_2 Composites for Efficient Photocatalytic Hydrogen Evolution. *J. Mater. Chem. A* **2014**, *2*, 3344–3351. [CrossRef]
35. Antoniadou, M.; Lianos, P. Near Ultraviolet and Visible Light Photoelectrochemical Degradation of Organic Substances Producing Electricity and Hydrogen. *J. Photochem. Photobiol. A Chem.* **2009**, *204*, 69–74. [CrossRef]
36. Daskalaki, V.M.; Antoniadou, M.; Li Puma, G.; Kondarides, D.I.; Lianos, P. Solar Light-Responsive Pt/CdS/TiO_2 Photocatalysts for Hydrogen Production and Simultaneous Degradation of Inorganic or Organic Sacrificial Agents in Wastewater. *Environ. Sci. Technol.* **2010**, *44*, 7200–7205. [CrossRef]
37. Strataki, N.; Antoniadou, M.; Dracopoulos, V.; Lianos, P. Visible-Light Photocatalytic Hydrogen Production from Ethanol-Water Mixtures Using a Pt-CdS-TiO_2 Photocatalyst. *Catal. Today* **2010**, *151*, 53–57. [CrossRef]
38. Chen, W.T.; Chan, A.; Sun-Waterhouse, D.; Moriga, T.; Idriss, H.; Waterhouse, G.I.N. Ni/TiO_2: A Promising Low-Cost Photocatalytic System for Solar H_2 Production from Ethanol-Water Mixtures. *J. Catal.* **2015**, *326*, 43–53. [CrossRef]
39. Strataki, N.; Bekiari, V.; Kondarides, D.I.; Lianos, P. Hydrogen Production by Photocatalytic Alcohol Reforming Employing Highly Efficient Nanocrystalline Titania Films. *Appl. Catal. B Environ.* **2007**, *77*, 184–189. [CrossRef]
40. López-Tenllado, F.J.; Hidalgo-Carrillo, J.; Montes, V.; Marinas, A.; Urbano, F.J.; Marinas, J.M.; Ilieva, L.; Tabakova, T.; Reid, F. A Comparative Study of Hydrogen Photocatalytic Production from Glycerol and Propan-2-Ol on M/TiO_2 Systems (M = Au, Pt, Pd). *Catal. Today* **2017**, *280*, 58–64. [CrossRef]
41. Dosado, A.G.; Chen, W.T.; Chan, A.; Sun-Waterhouse, D.; Waterhouse, G.I.N. Novel Au/TiO_2 Photocatalysts for Hydrogen Production in Alcohol-Water Mixtures Based on Hydrogen Titanate Nanotube Precursors. *J. Catal.* **2015**, *330*, 238–254. [CrossRef]
42. Pajares, A.; Wang, Y.; Kronenberg, M.J.; Ramírez de la Piscina, P.; Homs, N. Photocatalytic H_2 Production from Ethanol Aqueous Solution Using TiO_2 with Tungsten Carbide Nanoparticles as Co-Catalyst. *Int. J. Hydrogen Energy* **2020**, *45*, 20558–20567. [CrossRef]
43. Romero Ocaña, I.; Beltram, A.; Delgado Jaén, J.J.; Adami, G.; Montini, T.; Fornasiero, P. Photocatalytic H_2 Production by Ethanol Photodehydrogenation: Effect of Anatase/Brookite Nanocomposites Composition. *Inorganica Chim. Acta* **2015**, *431*, 197–205. [CrossRef]
44. Kontos, A.I.; Arabatzis, I.M.; Tsoukleris, D.S.; Kontos, A.G.; Bernard, M.C.; Petrakis, D.E.; Falaras, P. Efficient Photocatalysts by Hydrothermal Treatment of TiO_2. *Catal. Today* **2005**, *101*, 275–281. [CrossRef]
45. An, X.; Liu, H.; Qu, J.; Moniz, S.J.A.; Tang, J. Photocatalytic Mineralisation of Herbicide 2,4,5-Trichlorophenoxyacetic Acid: Enhanced Performance by Triple Junction Cu-TiO_2-Cu_2O and the Underlying Reaction Mechanism. *New J. Chem.* **2015**, *39*, 314–320. [CrossRef]

46. Shaban, M.; Poostforooshan, J.; Weber, A.P. Surface-Initiated Polymerization on Unmodified Inorganic Semiconductor Nanoparticles: Via Surfactant-Free Aerosol-Based Synthesis toward Core-Shell Nanohybrids with a Tunable Shell Thickness. *J. Mater. Chem. A* **2017**, *5*, 18651–18663. [CrossRef]
47. Cheng, J.; Wang, Y.; Xing, Y.; Shahid, M.; Pan, W. A Stable and Highly Efficient Visible-Light Photocatalyst of TiO_2 and Heterogeneous Carbon Core-Shell Nanofibers. *RSC Adv.* **2017**, *7*, 15330–15336. [CrossRef]
48. Guo, Y.; Zhang, L.; Liu, X.; Li, B.; Tang, D.; Liu, W.; Qin, W. Synthesis of Magnetic Core-Shell Carbon Dot@MFe_2O_4 (M = Mn, Zn and Cu) Hybrid Materials and Their Catalytic Properties. *J. Mater. Chem. A* **2016**, *4*, 4044–4055. [CrossRef]
49. Zeng, X.; Wang, Z.; Meng, N.; McCarthy, D.T.; Deletic, A.; Pan, J.H.; Zhang, X. Highly Dispersed TiO_2 Nanocrystals and Carbon Dots on Reduced Graphene Oxide: Ternary Nanocomposites for Accelerated Photocatalytic Water Disinfection. *Appl. Catal. B Environ.* **2017**, *202*, 33–41. [CrossRef]
50. Rangel-Mendez, J.R.; Matos, J.; Cházaro-Ruiz, L.F.; González-Castillo, A.C.; Barrios-Yáñez, G. Microwave-Assisted Synthesis of C-Doped TiO_2 and ZnO Hybrid Nanostructured Materials as Quantum-Dots Sensitized Solar Cells. *Appl. Surf. Sci.* **2018**, *434*, 744–755. [CrossRef]
51. Shathy, R.A.; Fahim, S.A.; Sarker, M.; Quddus, M.S.; Moniruzzaman, M.; Masum, S.M.; Molla, M.A.I. Natural Sunlight Driven Photocatalytic Removal of Toxic Textile Dyes in Water Using B-Doped ZnO/TiO_2 Nanocomposites. *Catalysts* **2022**, *12*, 308. [CrossRef]
52. Divyasri, Y.V.; Lakshmana Reddy, N.; Lee, K.; Sakar, M.; Navakoteswara Rao, V.; Venkatramu, V.; Shankar, M.V.; Gangi Reddy, N.C. Optimization of N Doping in TiO_2 Nanotubes for the Enhanced Solar Light Mediated Photocatalytic H_2 Production and Dye Degradation. *Environ. Pollut.* **2021**, *269*, 116170. [CrossRef]
53. Shi, R.; Li, Z.; Yu, H.; Shang, L.; Zhou, C.; Waterhouse, G.I.N.; Wu, L.Z.; Zhang, T. Effect of Nitrogen Doping Level on the Performance of N-Doped Carbon Quantum Dot/TiO_2 Composites for Photocatalytic Hydrogen Evolution. *ChemSusChem* **2017**, *10*, 4650–4656. [CrossRef]
54. Sargin, I.; Yanalak, G.; Arslan, G.; Patir, I.H. Green Synthesized Carbon Quantum Dots as TiO_2 Sensitizers for Photocatalytic Hydrogen Evolution. *Int. J. Hydrogen Energy* **2019**, *44*, 21781–21789. [CrossRef]
55. Hu, Z.; Shi, D.; Wang, G.; Gao, T.; Wang, J.; Lu, L.; Li, J. Carbon Dots Incorporated in Hierarchical Macro/Mesoporous g-C_3N_4/TiO_2 as an All-Solid-State Z-Scheme Heterojunction for Enhancement of Photocatalytic H_2 Evolution under Visible Light. *Appl. Surf. Sci.* **2022**, *601*, 154167. [CrossRef]
56. Girish, Y.R.; Udayabhanu; Alnaggar, G.; Hezam, A.; Nayan, M.B.; Nagaraju, G.; Byrappa, K. Facile and Rapid Synthesis of Solar-Driven TiO_2/g-C_3N_4 Heterostructure Photocatalysts for Enhanced Photocatalytic Activity. *J. Sci. Adv. Mater. Devices* **2022**, *7*, 100419. [CrossRef]
57. Guan, R.; Wang, L.; Wang, D.; Li, K.; Tan, H.; Chen, Y.; Cheng, X.; Zhao, Z.; Shang, Q.; Sun, Z. Boosting Photocatalytic Hydrogen Production via Enhanced Exciton Dissociation in Black Phosphorus Quantum Dots/TiO_2 Heterojunction. *Chem. Eng. J.* **2022**, *435*, 135138. [CrossRef]
58. Shi, F.; Xing, C.; Wang, X. Preparation of TiO_2/$MoSe_2$ Heterostructure Composites by a Solvothermal Method and Their Photocatalytic Hydrogen Production Performance. *Int. J. Hydrogen Energy* **2021**, *46*, 38636–38644. [CrossRef]
59. Huang, G.; Ye, W.; Lv, C.; Butenko, D.S.; Yang, C.; Zhang, G.; Lu, P.; Xu, Y.; Zhang, S.; Wang, H.; et al. Hierarchical Red Phosphorus Incorporated TiO_2 Hollow Sphere Heterojunctions toward Superior Photocatalytic Hydrogen Production. *J. Mater. Sci. Technol.* **2022**, *108*, 18–25. [CrossRef]